Petroleum Science 21 (2024) 2485–2501

Contents lists available at ScienceDirect

Petroleum Science

journal homepage: www.keaipublishing.com/en/journals/petroleum-science

Original Paper

Numerical evaluations on the fluid production in the in-situ conversion of continental shale oil reservoirs

Zhao-Bin Zhang [a, b, c, *], Maryelin Josefina Briceño Montilla [a, b, c], Shou-Ding Li [a, b, c, **], Xiao Li [a, b, c], Jian-Peng Xing [d], Yan-Zhi Hu [a, b, c]

[a] Key Laboratory of Shale Gas and Geoengineering, Institute of Geology and Geophysics, Chinese Academy of Sciences, Beijing, 100029, China
[b] Institute of Earth Sciences, Chinese Academy of Sciences, Beijing, 100049, China
[c] College of Earth and Planetary Sciences, University of Chinese Academy of Sciences, Beijing, 100049, China
[d] Institute of Energy, Peking University, Beijing, 100871, China

ARTICLE INFO

Article history:
Received 25 November 2023
Received in revised form
7 May 2024
Accepted 28 May 2024
Available online 29 May 2024

Edited by Meng-Jiao Zhou

Keywords:
In-situ conversion
Continental shale oil
Natural fracture network
TFC model

ABSTRACT

In-situ conversion presents a promising technique for exploiting continental oil shale formations, characterized by highly fractured organic-rich rock. A 3D in-situ conversion model, which incorporates a discrete fracture network, is developed using a self-developed thermal-flow-chemical (TFC) simulator. Analysis of the model elucidates the in-situ conversion process in three stages and defines the transformation of fluids into three distinct outcomes according to their end stages. The findings indicate that kerogen decomposition increases fluid pressure, activating fractures and subsequently enhancing permeability. A comprehensive analysis of activated fracture permeability and heating power reveals four distinct production modes, highlighting that increasing heating power correlates with higher cumulative fluid production. Activated fractures, with heightened permeability, facilitate the mobility of heavy oil toward production wells but hinder its cracking, thereby limiting light hydrocarbon production. Additionally, energy efficiency research demonstrates the feasibility of the in-situ conversion in terms of energy utilization, especially when considering the surplus energy from high-fluctuation energy sources such as wind and solar power to provide heating.

© 2024 The Authors. Publishing services by Elsevier B.V. on behalf of KeAi Communications Co. Ltd. This is an open access article under the CC BY license (http://creativecommons.org/licenses/by/4.0/).

1. Introduction

Continental shale oil is a type of liquid petroleum hydrocarbon extracted from continental oil shale formations that have not been buried deep enough to generate hydrocarbon through natural processes (Boak and Kleinberg, 2020). These formations contain a solid organic compound called kerogen, which serves as the precursor of oil and gas. Since kerogen can decompose into oil and gas when heated, the researchers suggested in-situ conversion as a potential technique to exploit these formations (Zhao et al., 2018). In-situ conversion is still an experimental technology, and there are many challenges to be overcome in terms of energy efficiency and environmental impact. Nonetheless, it holds promise to extract oil from shale formations that would be difficult or impossible to access with traditional drilling methods.

In China, there are at least five shale oil projecting basins: Ordos, Juggar, Sichuan, Songliao, and Bohai. These basins encompass highly prolific sections of source rock, containing organic matter at immature stages, including oil that has undergone conversion but not yet expulsion (He et al., 2020; Wang et al., 2021; Bai and Ma, 2020; Zhao et al., 2020; Zhu et al., 2019; Zou et al., 2020). These shale formations are naturally fractured, with early-stage thermal maturation often causing the formation of natural fractures (Meng et al., 2021; Zhang et al., 2017a, 2017b). Therefore, they serve as the primary storage for organic matter (Li et al., 2017; Zou et al., 2013). As the in-situ heating process begins, the temperature changes in the reservoir cause the kerogen bonds to break, releasing fluids that fill the free spaces and increase the pressure within the fractures. When the fluid pressure exceeds the tensile strength and normal closure stress of the fractures, a shear-slip movement occurs,

* Corresponding author. Key Laboratory of Shale Gas and Geoengineering, Institute of Geology and Geophysics, Chinese Academy of Sciences, Beijing, 100029, China.
** Corresponding author. Key Laboratory of Shale Gas and Geoengineering, Institute of Geology and Geophysics, Chinese Academy of Sciences, Beijing, 100029, China.
E-mail addresses: zhangzhaobin@mail.iggcas.ac.cn (Z.-B. Zhang), lsdlyh@mail.iggcas.ac.cn (S.-D. Li).

https://doi.org/10.1016/j.petsci.2024.05.025
1995-8226/© 2024 The Authors. Publishing services by Elsevier B.V. on behalf of KeAi Communications Co. Ltd. This is an open access article under the CC BY license (http://creativecommons.org/licenses/by/4.0/).

leading to an improvement in reservoir permeability (Gischig and Preisig, 2015).

In the past years, the studies on in-situ conversion focused primarily on the injection models carried out by Shell in the Green River Formation (Fowler and Vinegar, 2009). For instance, Brandt (2008) modeled the in-situ conversion process (ICP) of Shell and revealed that the energy outputs are 1.2–1.6 times greater than the total energy inputs. However, the greenhouse emissions are 20% larger than the conventionally produced petroleum. Shen (2009) simulated the heating and production process of the Mahogany field experiments with the commercial software CMG-STARS (CMG Software | STARS, 2023). They identified heat loss through wellbore flows and its impact on production. Hazra (2014) conducted an analysis of different heating schemes and configurations using the CMG-STARS. They performed a sensitivity analysis to compare the energy efficiency of various in-situ retorting technologies. In 2023, Huang et al. (2023) developed a thermo-hydro-mechanical-chemical model to investigate the mechanism and influence of engineering parameters in in-situ conversion. Their simulation utilized the Shell ICP injection scheme and demonstrated significant changes in reservoir stress during the heating process. However, none of these models attempted to account for the effects of natural fractures on permeability, either before or after kerogen decomposition, despite their prevalence in continental oil shale formations (Ryan et al., 2010). Fan et al. (2010) conducted a sensitivity analysis of the Shell ICP but only developed a non-fractured reservoir model with high permeability to represent natural fractures. Lee et al. (2015) on the other hand, expanded the Texas A&M University Flow and Transport Simulator (Thoram and Ehlig-Economides, 2011) to include kerogen pyrolysis. This study incorporated a fracture domain to represent natural fractures, but it mainly focused on sensitivity analysis related to fracture spacing. Additionally, Egboga et al. (2017) examined thermal stimulation to improve oil recovery in shale reservoirs during early-stage depletion. However, their consideration of micro-fractures was relatively simplistic, pre-setting effective permeability and effective width. In this regard, it is observed that the studies on in-situ conversion have explored the impacts of various factors, such as energy efficiency and heating schemes, however, there has been a notable absence of consideration for natural fractures in these models. Those play a crucial role in reservoir permeability, and it should be accounted for to enhance the accuracy and applicability of in-situ conversion techniques.

These analyses also focus primarily on the study of the in-situ conversion technique itself and do not adequately address the availability of energy sources necessary to make this technique feasible. Especially, considering that the continuous injection of heat for conversion over extended periods indicates substantial energy demands, resulting in high-energy consumption. Nonetheless, studies by Shi et al. (2023) suggest that while initial high-energy utilization efficiency during kerogen pyrolysis may seem promising, it diminishes significantly over time due to inefficient heating practices, highlighting the phenomenon of useless heating. In this context, despite its energy-intensive nature, in-situ conversion exhibits minimal demands for power supply stability. Consequently, leveraging high power fluctuations from solar and wind sources for in-situ conversion emerges as a viable strategy. This alternative approach not only introduces the possibility of utilizing shale oil reservoirs for energy storage but also presents a promising avenue for improving sustainability and reducing costs in oil shale exploitation processes.

In this study, assuming that the integration of renewable energy can make in-situ conversion more sustainable and economically viable, this article presents a thermo-fluid-chemical (TFC) model that incorporates fractures. To begin, the new algorithm and heat injection system are introduced, and a three-dimensional heterogeneous model is established on this basis. Using this model, the evolution processes of fracture activation, temperature, pressure field, and various phase saturation during in-situ heating are analyzed. Given the complexity of modeling heterogeneity of the shale oil reservoir, the impact of two key factors on the development process: the permeability of the activated fracture and heating power is analyzed comprehensively. Subsequently, an optimization scheme is proposed, addressing both development efficiency and energy utilization efficiency.

2. Methods

In-situ conversion is a complex process that encompasses multiphase and multicomponent flow, heat transfer, chemical reactions, and the activation of natural fractures. Simulating all the detailed processes involved is challenging. Given the high density of natural fractures in shale reservoirs, the analysis focus primarily lies on evaluating the permeability of these fractures activated in shale oil development. Furthermore, it is assumed that the model comprises five distinct phase states: gas, water, light oil, heavy oil, and solid. Within the gas phase, two components are identified: water steam and methane. In the solid phase, two components, kerogen and coke, are recognized. It should be noted that the solids are considered special fluids with infinite viscosity. Notably, heavy oil and light oil are treated as separate phases. By considering them as separate phases rather than components within the same phase, the model can better capture their distinct flow behaviors and accurately represent their flow resistances based on saturation and relative permeability.

2.1. Thermal-flow-chemical model

This research employs a comprehensive simulation approach to model the in-situ conversion process, utilizing our self-developed thermal-flow-chemical (TFC) coupling simulator (accessible at IGG-Hydrate: https://gitee.com/geomech/hydrate), which has demonstrated successful application in previous studies (e.g., Xu et al., 2021; Briceño M. et al., 2023; Zhang et al., 2023, 2024). Here below we provide a brief overview of the models and equations involved in the in-situ conversion process.

The simulation of multiphase flow constitutes the main thread of the entire model, given that the simulation aims to assess the production capacity of oil and gas. It is assuming that the flow of each fluid phase follows Darcy's law (Darcy, 1856):

$$\boldsymbol{v}_\alpha = \frac{k k_{\mathrm{r},\alpha}}{\mu_\alpha}\left(-\nabla p_\alpha + \rho_\alpha \boldsymbol{g}\right) \tag{1}$$

where $\boldsymbol{v}$ is the Darcy velocity in m/s, k is the intrinsic permeability in mD, k_r is the relative permeability, μ is the fluid dynamic viscosity in Pa·s, p is the fluid pressure in Pa, ρ is the fluid density in kg/m^3, and $\boldsymbol{g}$ is the gravity vector in m/s^2. The subscript α represents the fluid phases, which includes gas, water, light oil, heavy oil, and solid. For simplification purposes, both density ρ and viscosity coefficient μ are functions of fluid temperature and pressure, and it supposes that $k_{\mathrm{r},\alpha}$ is a function of saturation s_α.

Based on Briceño M. et al. (2023) and Zhang et al. (2023), mass conservation applies as follow:

$$\frac{\partial \phi \rho_\alpha s_\alpha}{\partial t} = -\mathrm{div}(\rho_\alpha \boldsymbol{v}_\alpha) \tag{2}$$

where ϕ is the porosity, t is time in s, s_α is the volume fraction of phase α, and the sum of the saturations of all phases in a pore is

unity.

$$\sum_{\alpha} s_{\alpha} = 1 \tag{3}$$

Heat transfer involves two fundamental processes: conduction and convection. Conduction refers to the transfer of heat due to temperature differences, while convection, often the dominant mechanism, involves the fluid itself carrying heat and inducing fluid flow. By analyzing the current fluid flow conditions, the model calculates heat transfer, encompassing both conduction and convection processes.

$$\boldsymbol{q}_{\text{heat}} = -\lambda \nabla T + \sum_{\alpha} (\rho_{\alpha} c_{\alpha} \boldsymbol{v}_{\alpha} T) \tag{4}$$

where $\boldsymbol{q}_{\text{heat}}$ is the heat flow, c is the specific heat in J/(kg·K), λ is the thermal conductivity in W/(m·K), T is the temperature in K. According to the principle of conservation of energy, the change of temperature depends on the heat transfer:

$$\text{div}\boldsymbol{q}_{\text{heat}} = -\left[\phi \sum_{\alpha} \sum \rho_{\alpha} c_{\alpha} s_{\alpha} + \rho_{\text{s}} c_{\text{s}}\right] \frac{\partial T}{\partial t} \tag{5}$$

where ρ_{s} and c_{s} represent the bulk density in kg/m^3 and the specific heat of the porous media in J/(kg·K), respectively.

In the context of chemical reactions, the focal point here revolves around the decomposition of components after being heated. It is crucial to acknowledge that the importance of reaction kinetics varies depending on the scale of the processes in question. For reactions conducted at the laboratory scale, which typically unfold over minutes or hours, a comprehensive grasp of kinetics is of paramount importance. However, when scrutinizing in-situ scenarios at the reservoir scale, where development can span a decade or more, the significance of the reaction process diminishes. Therefore, for this research, which centers on reservoir-scale and multi-year development, an equilibrium reaction model to encapsulate the decomposition process is employed.

For the decomposition of components, it sets the existence of a critical temperature T_{eq}, such its decomposition only occurs when the temperature T exceeds T_{eq}. The decomposition process consumes heat, causing a decrease in temperature. When the temperature drops below T_{eq}, the decomposition ceases. By utilizing this approach, it becomes convenient to compute the masses of components involved in reactions based on the temperature within each grid cell.

To compute the thermal-flow-chemical coupling process, an explicit method is applied. At first, the thermal-flow-chemical framework is set defining the essential fluid properties and chemical reactions to establish a comprehensive computational model. Next, the calculation process in one step unfolds as follows.

1) Disregarding the heat conduction and chemical reactions, the multiphase multicomponent flow and the heat convection processes are calculated.
2) The heat conduction is computed, therefore, the temperature within each grid cell is updated.
3) The reactions within each grid cell are computed. This allows updating the mass of each component within each grid cell, as well as the cell's temperature.

2.2. Fluids and reactions

Based on the thermal-flow-chemical coupling framework, a computational approach is established by incorporating fluids and reactions during in-situ conversion. In the context of multiphase flow, the relative permeability plays a vital role in determining the resistance of each phase. However, acquiring relative permeability data is notably challenging, particularly due to the presence of five fluid phases in our model. For the sake of simplification, a modified version of Stone's relative permeability method is employed for all fluid phases (Stone, 1970). This approach simplifies the modeling process by allowing the relative permeability of each fluid phase to be calculated based on its saturation.

$$k_{\text{r},\alpha} = \left(\frac{s_{\alpha} - s_{\text{ir},\alpha}}{1 - s_{\text{ir},\alpha}}\right)^{n_{\alpha}} \tag{6}$$

where the residual saturation s_{ir} is set to 0.05, and the reduction exponent n_{α} is fixed at 3.0.

In the case of various fluids involved in the model, density stands as one of the most fundamental properties of fluids. The density of methane gas is considered as a function of pressure and temperature. The data provided by Younglove and Ely (1987) is used, which has been fitted to the range employed in the simulations:

$$\rho_{\text{g}} = \frac{M_{\text{m}} p_{\text{g}} \times 10^6}{RT}\left(1.0 + 0.025 p_{\text{g}} - 0.000645 {p_{\text{g}}}^2\right) \tag{7}$$

where ρ_{g} is the density of methane gas in kg/m^3, $R = 8.314$ J/(mol·K) is the gas constant, $M_{\text{m}} = 0.016042$ kg/mol is the molecular mass of methane, p_{g} is the gas pressure in MPa, and T is the temperature in K. The density of water steam is obtained from the International Association for the Properties of Water and Steam tables (IAPWS-IF97) (Wagner and Kretzschmar, 2019).

During the in-situ conversion, the change of fluid volume is mainly controlled by the decomposition process and the density change of gas phase. By contrast, the density changes of liquid and solid phases are ignorable. Therefore, it is assumed that liquids and solids are incompressible and assign them fixed densities. Specifically, $\rho_{\text{water}} = 985.8$ kg/m^3, $\rho_{\text{heavy oil}} = 980$ kg/m^3, $\rho_{\text{light oil}} = 797.2$ kg/m^3 (Lei et al., 2016), $\rho_{\text{kerogen}} = 2590$ kg/m^3 and $\rho_{\text{coke}} = 1100$ kg/m^3 (Zhao et al., 2021; Coal-Classification, 2023).

The viscosity of a fluid determines the resistance to fluid flow, making it a critical factor in the assessment of productivity. The viscosity of methane gas μ_{g} is assumed dependent on both pressure and temperature, and the fitted equation by Younglove and Ely (1987) is used:

$$\mu_{\text{g}} = 10.3 \times 10^{-6} \exp\left[1 + 0.053 p_{\text{g}} \left(\frac{280}{T}\right)^3\right] \tag{8}$$

where μ_{g} is the viscosity of methane gas in Pa·s.

The viscosity of the water and water steam are adopted according to the correlations for industrial applications of the International Association for the Properties of Water and Steam given by Wagner and Kretzschmar (2019). And to define the viscosity of heavy oil and light oil, the Yaw's handbook of thermodynamic and physical properties of chemical compounds is used (Yaws, 2003):

$$\mu_{\text{oil}} = 10^{a + \frac{b}{T} + cT + dT^2 - 3} \tag{9}$$

where μ_{oil} is the viscosity of oil in Pa·s; the coefficients a, b, c, d are defined according the fluids, for light oil are -5.0206, 894.52 K, 0.0096 K^{-1}, and -9.8×10^{-6} K^{-2}; and for heavy oil are -4.5109, 1184.7 K, 0.0062 K^{-1}, and -5.4491×10^{-6} K^{-2}.

Finally, to complete the configuration, attention must be given to the chemical reactions between components. Although heavy oil, light oil, and natural gas consist of mixtures with multiple components, this model assumes that they primarily consist of docosane ($C_{22}H_{46}$), undecane ($C_{11}H_{24}$), and methane (CH_4), respectively.

The decompositions of kerogen and heavy oil are considered a modification from Braun and Burnham (1993) and Lee et al. (2015). The model simplifies the decomposition of kerogen into two liquid hydrocarbons and gas, followed by heavy oil decomposing into light oil, gas, and coke as Eq. (10). Additionally, the appearance of water and only one type of coke are considered. The mass stoichiometry factors are based on the kerogen decomposition from Burnham and Braun (1985) and Braun and Burnham (1993), as well as laboratory experiment observations (e.g., Guo et al., 2022; Pei et al., 2020; Turakhanov et al., 2021; Wang et al., 2022). To enable kerogen and heavy oil decomposition, it requires enough heat injection to surpass the minimum energy barrier between reactants and products, which is defined by the activation energy and the temperature of decomposition. In this regard, those values are adopted based on Lee (2014). Thus, the activation energy for both following reactions is 161.6 kJ/mol and 206.0 kJ/mol, while corresponding reaction temperatures are 565 K and 603 K, respectively.

$$\text{Kerogen} \rightarrow 0.6C_{22}H_{46} + 0.1C_{11}H_{24} + 0.1CH_4 + 0.1H_2O + 0.1\text{Coke} \tag{10}$$

$$C_{22}H_{46} \rightarrow 0.5C_{11}H_{24} + 0.2CH_4 + 0.3\text{Coke} \tag{11}$$

In the model, the intricate dynamics of water phase transition are meticulously considered, particularly as temperature increase. This aspect is captured by modeling the phase transitions of vaporization and condensation of water, governed by their enthalpy changes and temperature thresholds. To precisely define the occurrence and mechanism transition, the Antoine equation is employed to characterize vapor pressure as a function of local temperature (Thomson, 1946).

2.3. Fractures

In continental shale formations, natural fractures often exhibit significant development, rendering their consideration crucial for evaluating productivity. Since the primary role of natural fractures is to serve as conduits for fluid flow, and the objective of this study is to assess fluid production during in-situ conversion processes, the focus lies primarily in considering the influence of natural fractures from a fluid flow perspective. Initially, it is assumed the presence of natural fractures in a cemented state or filled with organic matter. However, when fluid pressure surpasses certain thresholds, these fractures become activated, thereby increasing the permeability and providing additional seepage pathways. When an activated fracture intersects a grid cell, the increase in permeability due to the activated fracture, as governed by the cubic law of flow within the fracture, can be expressed as a modification described by Li et al. (2021):

$$\Delta k = \frac{w^3}{12L} \tag{12}$$

where w represents the hydraulic aperture of the activated fracture, and L is the characteristic scale of the grid cell.

During the in-situ conversion process, the aperture of fractures undergoes variations and their conductivity increases upon activation. The activation of fractures in unconventional reservoirs constitutes a complex fluid-rock coupling process, which has been extensively explored (e.g., Wang et al., 2023). However, when the number of fractures exceeds several thousand, the computational demands for stress and fracture activation become immense. For the sake of simplification, it is assumed that all open fractures have the same aperture in this work. To assess the conditions for natural fracture activation, we consider a set of mutually parallel infinitely long activated fractures with spacing d and aperture w, the stress is given by

$$\sigma_n = \sigma_0 + \frac{wE}{d} \tag{13}$$

Here E represents the elastic modulus of the rock, and σ_0 is the initial stress. Assuming the tensile strength of the fractures is σ_c, the critical fluid pressure required for a new fracture to open is

$$p_c = \sigma_0 + \sigma_c + \frac{wE}{d} \tag{14}$$

When there are many random fractures, it is difficult to calculate the fracture spacing accurately. In such cases, it approximates as

$$d \approx \frac{1}{P_{32}} \tag{15}$$

Here P_{32} represents the total fracture area per unit volume, characterizing fracture density. Substituting this formula into the previous equation, it obtains

$$p_c \approx \sigma_0 + \sigma_c + P_{32}wE \tag{16}$$

Thus, the critical pressure for fracture activation is linearly related to the density of already activated fractures. Specifically, when $p > \sigma_0 + \sigma_c$, the first fracture will activate, and as fluid pressure increases, more fractures will activate. The number of newly activated fractures is directly proportional to the increase in pressure. Consequently, during model setup, a critical fluid pressure is assigned to each fracture, and during computation, when the fluid pressure exceeds this critical value, the fracture is set to an open state, and the permeability of the grid cells intersected by the activated fracture is increased accordingly.

2.4. Verification

This research presents multiphase and multicomponent models, which were initially validated through heat flow coupling simulations, classical models, and laboratory experiments (Xu et al., 2021; Zhang et al., 2023). By incorporating kerogen and heavy oil decomposition, the validation of the decomposition model is necessary. In this work, basic validation is conducted using a classical heavy oil decomposition experiment conducted by Pei et al. (2020).

Using the TFC coupling model established above, and without considering natural fractures, a core scale in-situ conversion model is developed. The model settings are depicted in Fig. 1(a). The experiment configuration consists of heavy oil whose density is 1007 kg/m^3, viscosity is 191.6 Pa·s, the mass of the sample is 0.02 kg, the reactor initial temperature is 599.15 K, and reactor pressure is 3.2 MPa. The kinetic parameters consist of the thermal decomposition of heavy oil in 0.1807 of gas, 0.5738 of light oil, and 0.2455 of coke (expressed in mass stoichiometric factors). Following the experiment settings, the temperature of decomposition of heavy oil is set over 623.15 K with a rate constant reaction of 1.21×10^6 s^{-1}. During the calculation process, the mass of the components is recorded at the outlet position which simulation results are shown in Fig. 1(b). The result demonstrates good agreement with the experimental data. The cracking rate fits with

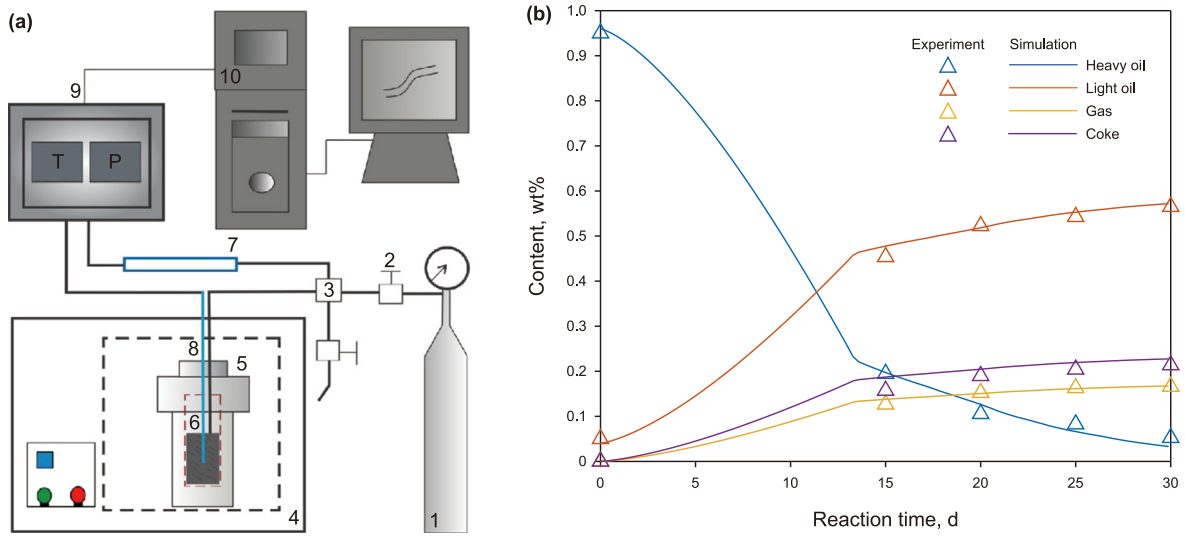

Fig. 1. **(a)** The schematic diagram of equipment used for thermal cracking experiments given by Pei et al. (2020): (1) high-pressure gas bottle (air or nitrogen), (2) valve, (3) four-way connection, (4) digital-controlled thermo-oven, (5) high pressure stainless-steel reactor, (6) oil sample, (7) pressure sensor, (8) temperature sensor, (9) data acquisition system, and (10) computer. **(b)** Simulation and experiment values results of oil components. The triangles in the graph represent experimental data obtained after the thermal cracking of ultra-heavy oil in the presence of nitrogen. This data serves as part of the verification model alongside air injection, as illustrated by Briceño et al. (2023).

the experiment data, and the appearance of the mass products conforms closely to the stoichiometric equation. These findings affirm the reliability of the proposed thermal-flow-chemical model.

3. Model

3.1. Heating scheme

An important issue in in-situ conversion methods is the substantial energy consumption during the heating stage. Therefore, utilizing conventional electrical energy for heating is undoubtedly wasteful, which constitutes a primary reason for the skepticism surrounding in-situ conversion (Brandt, 2008). Fortunately, the regions where China's main shale oil reservoirs are located possess abundant solar and wind energy resources (Wang et al., 2022; Yang et al., 2019). Solar and wind energy are characterized by significant fluctuations, making their direct integration into the power grid challenging. Consequently, harnessing surplus solar and wind energy from peak generation periods and utilizing it for reservoir heating—a process depicted in Fig. 2—can significantly reduce the costs of in-situ conversion. On the surface, the excess energy that cannot be utilized for wind and solar power generation is directly injected into the reservoir for heating. Within the reservoir, heating elevates the reservoir temperature, causing kerogen and heavy oil to decompose, increasing reservoir pressure, activating fractures, and resulting in oil and gas production. In the following sections, it will establish a numerical model based on this concept for further analysis.

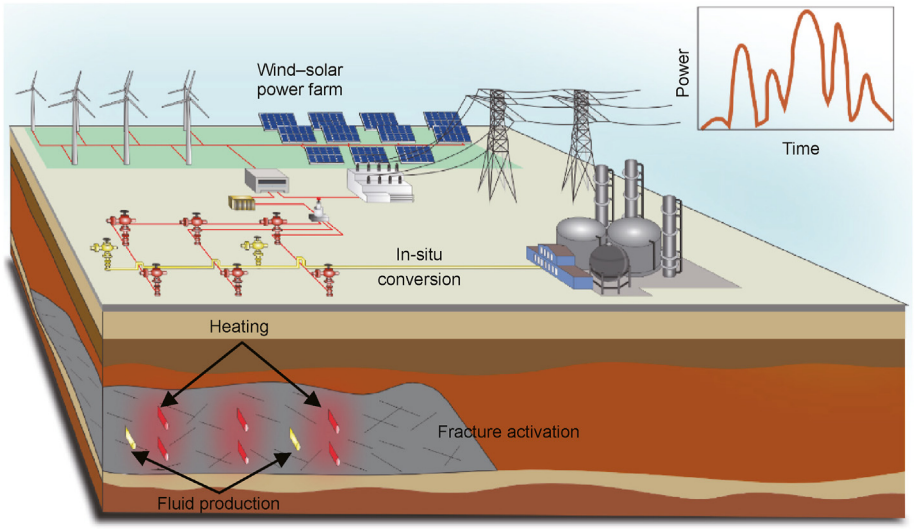

Fig. 2. Schematic representation of in-situ shale oil conversion. The injected energy is derived from wind and solar sources characterized by pronounced fluctuations that prevent their integration into the conventional power grid as unused wasted energy. The inset in the upper right corner illustrates a typical energy fluctuation curve for solar energy throughout the day. Within the shale oil reservoir, a network of horizontal wells is employed for heating and production, with red denoting heating wells and yellow representing production wells.

3.2. Natural fractures

Natural fractures in continental shale are often well developed due to thermal maturation (Meng et al., 2021). These fractures play a crucial role in storing organic material (Li et al., 2017; Zou et al., 2013) and in improving the permeability of the reservoir (Gischig and Preisig, 2015; Zhang et al., 2017c). Therefore, the direction and density of fractures are critical to the development of shale oil and gas. The Chang 7 member is well suited for the in-situ conversion process due to its organic-rich shales of low and medium thermal maturity, and the occurrence of delamination, which enables the formation of microfractures (Fu et al., 2018; Hu et al., 2020; Jia et al., 2016). The discrete fracture network for the Chang 7 shale is built based on fractures obtained from outcrops and downhole cameras collected in the Weibei uplift zone of the Ordos Basin (Li et al., 2021). This data is used to create a 3D fracture network model of the shale gas reservoir that accounts for both the bedding structure and natural fractures.

3.3. Model settings

In this research, the simulation model is a three-dimensional model that comprises four horizontal wells containing electrical heaters, and a horizontal producer well maintained at a constant pressure of 3.0 MPa. The discrete fracture network (DFN) model for the Chang 7 shale is built based on fractures obtained from outcrops and downhole cameras (Fig. 3(a)). Initial saturation, organic matter content, and porosity data for the Chang 7 member are established based on the research conducted by Zhao et al. (2018) (see Fig. 3(c)). Their findings reveal that the effective thickness of the Chang 7 member is less than 20 m. Consequently, using our self-developed simulator, a regular mesh grid is created, resulting in a 3D model measuring 15 m $\times$ 10 m $\times$ 15 m; with a resolution of 60 $\times$ 10 $\times$ 60 grids in the x, y, and z directions respectively (see Fig. 3(b)). It must be pointed out here that the small-scale model can be regarded as a small part of a larger-scale model. Around, above, and below this model, similar models can be considered adjacent. Therefore, considering the periodicity or symmetry of the model in three directions, both the surrounding, upper, and lower boundaries are set as fluid-closed and adiabatic boundaries, and the input data of initial condition and reservoir properties are listed in Table 1. It is important to note that, although waste energy is used for heat injection, the input power exhibits significant fluctuations. However, due to the multi-year duration of the heat injection process, these short-term fluctuations can be considered negligible. Therefore, in this study, a constant injection power is still employed in the heat injection calculations.

4. Results and discussions

4.1. TFC coupling evolution processes

The in-situ conversion of continental shale oil is a thermal-flow-chemical coupling process, a consensus within the academic community. However, the precise nature of this coupling evolution during in-situ conversion and the distinctive characteristics exhibited by the fluid, solid, heat transfer, and reaction phenomena remains unclear based on our literature review. Therefore, this study intends to employ the model established in the previous section to calculate and elucidate the spatiotemporal evolution patterns of various physical fields during the in-situ conversion, addressing this critical gap in understanding. In this research, it is simulated a 10-year development period under constant heating power and constant production pressure. Through comprehensive analysis of this 10-year process, it becomes evident that the entire lifecycle of in-situ conversion progresses through three distinct stages.

1) *Heating stage.* This stage is characterized mainly by the continuous increase in reservoir temperature while the reservoir pressure undergoes slight variations. The temperature gradually increases from the injection well, spreading throughout the reservoir while remaining below the critical temperature at which kerogen and heavy oil decompose. Consequently, the overall impact on reservoir pressure remains relatively minor during this stage. This is primarily attributed to the predominant influence of material decomposition in overall reservoir pressure. Such stability in pressure distinguishes the heating stage from the subsequent stages of the process; and based on the calculated parameters, this lasts for approximately 4 years (Fig. 4(a)).
2) *Reaction stage.* The main feature of the reaction stage is the rapid increase in fluid pressure. During the heating stage, the reservoir gradually reaches the critical temperature at which kerogen decomposes, and the hydrocarbon is released (Espitalie et al., 1977). During this stage, the injection well continues to provide heat, and the excess energy causes the cracking of kerogen and heavy oil into lighter oil, natural gas, water, and other lower-density components. In addition, a simultaneous vaporization of liquid water occurs. As the volume of fluid increases, it leads to a rise in fluid pressure within the pores and fractures (Xi, 2022). Consequently, numerous fractures are activated (Gischig and Preisig, 2015). As a result, the fracture's permeability increases following the established model configuration. Based on the calculated parameters, as shown in Figs. 4(b) and 5, the reaction stage lasts for approximately 2 years.
3) *Production stage.* In this stage, the continuous decrease in fluid pressure takes precedence. This is due to the activation of fractures enhancing their permeability, allowing heavy oil, light oil, natural gas, and other fluids to be produced from the production wells, resulting in a decrease in reservoir fluid pressure (Wang et al., 2023). Therefore, the elastic energy in the reservoir matrix and fluids is depleted, and fluid pressure decreases to the same level as in the production wells, consequently, the fluid production ceases. During this stage, the viscosity of dense fluids, such as heavy oil, decreases. Therefore, their production increase in comparison to other fluids.

It is worth noting that the three stages defined here do not have strict and clear time boundaries. In the heating phase, near the injection well, where the temperature rises rapidly, component decomposition may occur. During the reaction phase, fluid production can begin as fluid pressure increases and/or temperature increases reach the production well. In the production phase, there may still be some partially remaining kerogen and heavy oil undergoing continued decomposing.

Throughout the entire in-situ conversion process, the reservoir undergoes a transition from its initially stable state. The heating of the injection well and the opening of the production well lead to complex phenomena, with components undergoing decomposition, resulting in the release of light fluids and their subsequent production. Eventually, the reservoir returns to a stable state. During the entire process, it is observed that there are approximately three end stages for fluids within the reservoir.

1) *Thermal decomposition.* After a sufficiently long period of continuous heating, nearly all components thermally vulnerable in the reservoir, including kerogen and heavy oil, will eventually decompose. In Fig. 6(a), it can be observed that the kerogen mass in place decreases rapidly, indicating a consistent pattern

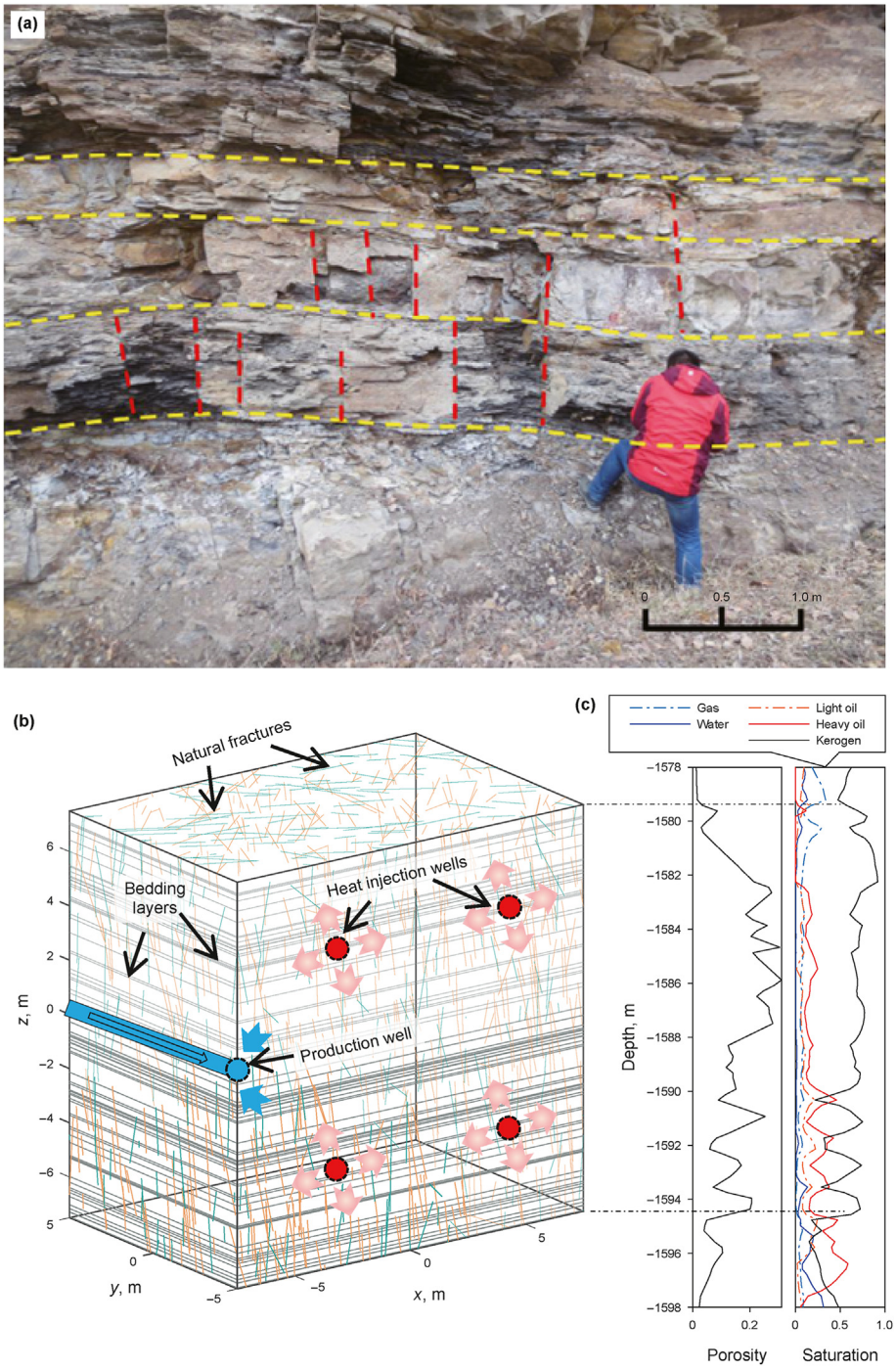

Fig. 3. **(a)** Fracture mapping from the outcrops collected in the Weibei uplift zone of the Ordos Basin (Li et al., 2021); **(b)** distribution map of natural cracks (based on Li et al. (2021)); **(c)** geological profile of Chang 7 (data processing according to Zhao et al. (2018)).

with the verification work conducted by Lee (2014); the average saturation of kerogen reaches nearly half of the initial saturation after 5 years of treatment, and complete decomposition is achieved after 7 years approximately. On the other hand, the mass of heavy oil in the reservoir ultimately tends towards zero (Fig. 6(b)). This is partly due to the flow and production of heavy oil due to the improvement of permeability (Fig. 7(a)). However, the role of heavy oil cracking should not be overlooked; without cracking, a significant amount of heavy oil residue would inevitably remain in the pores, and there would be less light oil available to produce.

2) *Fluid production.* The production of fluid hydrocarbons such as heavy oil and light oil depends on their susceptibility to decomposition, their nature, and reservoir characteristics. For gases, or fluids prone to transforming into gas-like forms (such as water), due to their low viscosity, it is possible to achieve almost total fluid production. Notably, the duration of gas production, as depicted in Fig. 7(b), is distinctively longer when compared to other fluids and gases. This extended production duration can be attributed to the expulsion of gases resulting from the cracking of heavy oil and kerogen. Conversely, the production of water and water steam is more limited, influenced

Table 1
Input parameters used in simulation model.

Parameters	Value
Initial conditions	
Initial temperature	338 K
Initial pressure	20.0×10^6 Pa
Well producer pressure	3.0×10^6 Pa
Power heating	20 kW
Reservoir properties[a]	
Matrix permeability	0.01 mD
Activated fracture's permeability (AFP)	1.0 mD
Rock density	2500 kg/m^3
Rock heat conductivity	2.0 J/m·K
Rock heat capacity	2000 J/kg·K

[a] (Dang et al., 2016; Wood, 2022; Xue et al., 2019).

by the rise in temperature. Consequently, the quantity of the gas phase that ultimately remains in the reservoir is relatively low.

3) *Residue in pores.* Firstly, the coke generated after the decomposition of kerogen and heavy oil, being a solid fluid, will all remain in place. Remarkably, for light oils, which demand higher temperatures for effective cracking, a substantial quantity of oil can be extracted during the treatment process (Fig. 6(c) and (d)). However, simultaneously, a significant portion of oil remains trapped within the reservoir pores. This is due to the direct effect of increased permeability on the production of fluids. The accelerated flow and rapid drainage, facilitated by increased permeability, promote a reduction in pressure, depleting the reservoir's energy reserves. As a result, the drainage of light oil becomes less efficient over time. Therefore, it can be concluded that given a sufficiently extended treatment period, the predominant composition of the residual oil within the pores will largely consist of light oil.

It should be noted that after prolonged heating and production, the end stages of fluids might not be unique. For example, heavy oil may either be cracked or produced directly as a fluid. Similarly, light oil can be both produced as a fluid and have a portion remaining in the pores.

In summary, in this section, an analysis of the geological features of the Chang 7 formation and calculated the in-situ conversion process under a constant heating power of 20 kW was conducted.

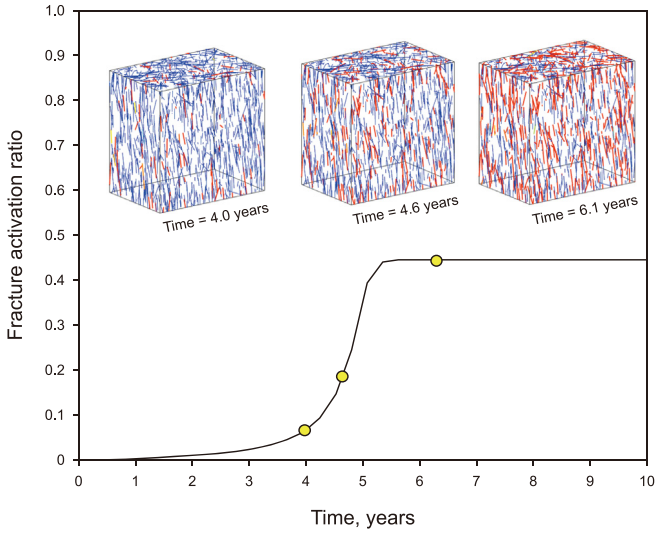

Fig. 5. Curve depicting the temporal evolution of natural fracture activation proportion within the reservoir during in-situ conversion. The activation proportion of natural fractures is defined as the ratio between the number of activated natural fractures and the total number of fractures. The three small insets in the figure represent the state of fracture activation corresponding to the moments marked by circles on the curve, with red denoting activated fractures and blue representing natural fractures that remain inactive.

Here, three distinct stages in the entire lifecycle of in-situ conversion and three possible outcomes for reservoir materials were identified. However, since in situ conversion is a typical thermo-fluid coupled process, both fluid flow and heat injection can have an impact on chemical reactions and production. Depending on the reservoir permeability and heating power conditions, the in-situ conversion process may exhibit varying characteristics. Therefore, based on the calculations presented in this section, permeability, and heating power are adjusted to investigate their influence on the in-situ conversion process.

4.2. Effects of activated fracture's permeability

Due to the low permeability of the shale matrix, in the case of

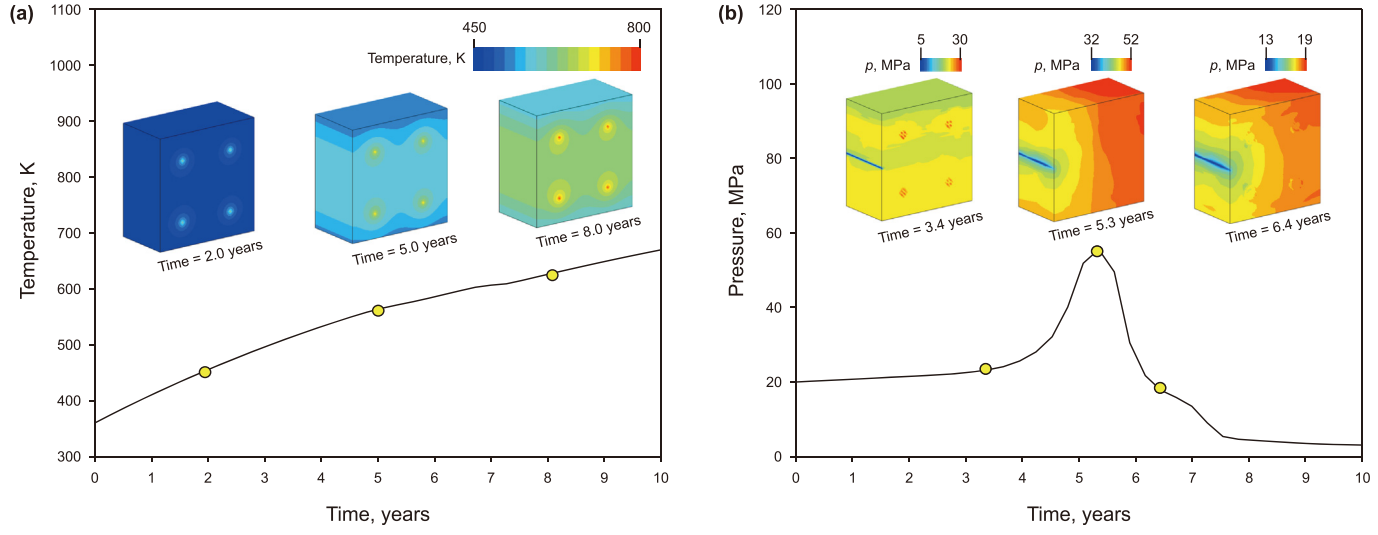

Fig. 4. Temporal and spatial evolution of reservoir **(a)** temperature and **(b)** pressure during in-situ conversion. The curves in the figure represent the average temperature or pressure within the reservoir, while the insets depict three-dimensional temperature or pressure fields corresponding to the moments marked by circles on the curves.

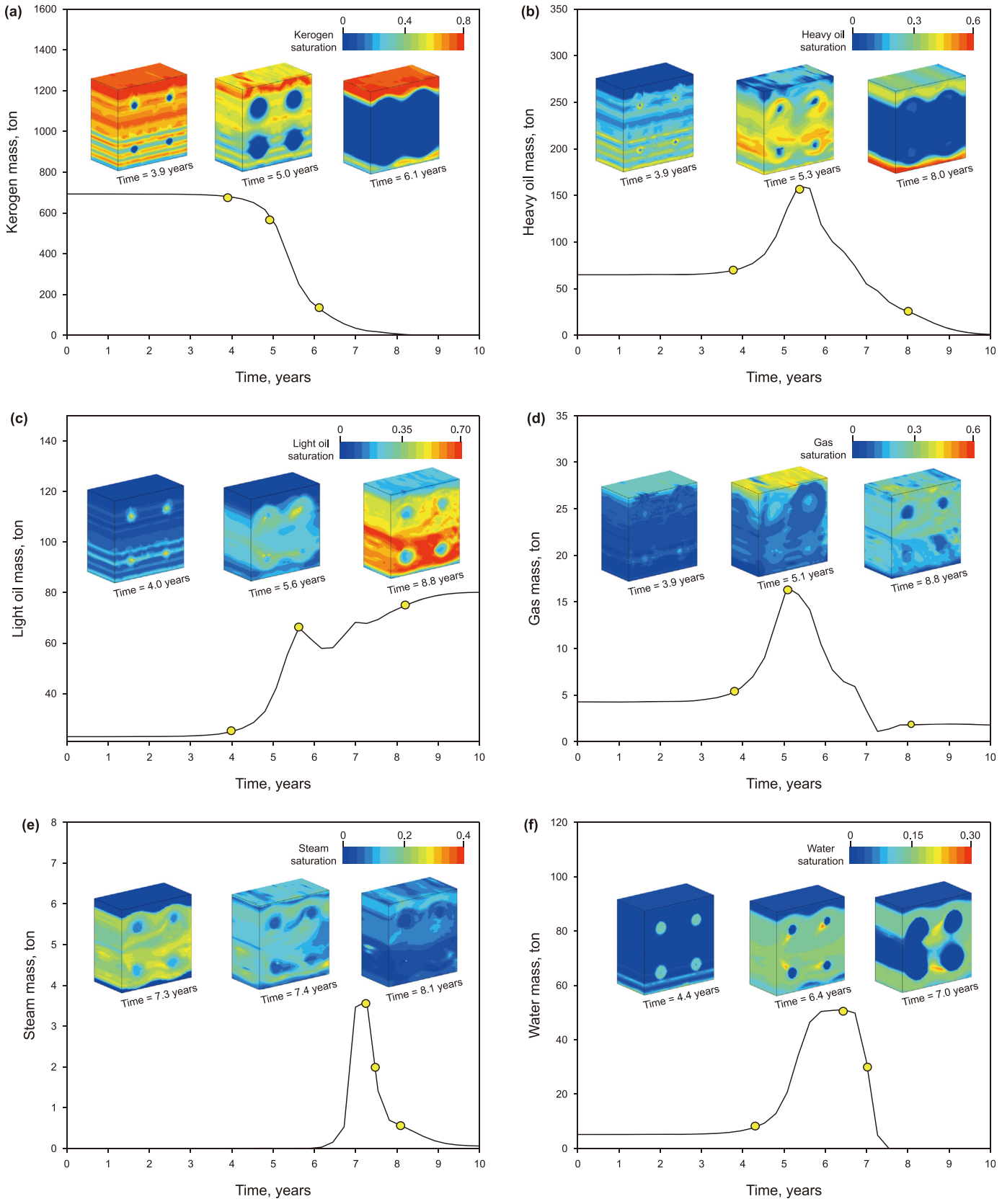

Fig. 6. Temporal evolution curves of reservoir **(a)** kerogen mass, **(b)** heavy oil mass, **(c)** light oil mass, **(d)** methane gas mass, **(e)** steam mass, and **(f)** water mass during in-situ conversion. The small insets within each graph depict the three-dimensional saturation fields of the fluids corresponding to the moments marked by circles on the curves.

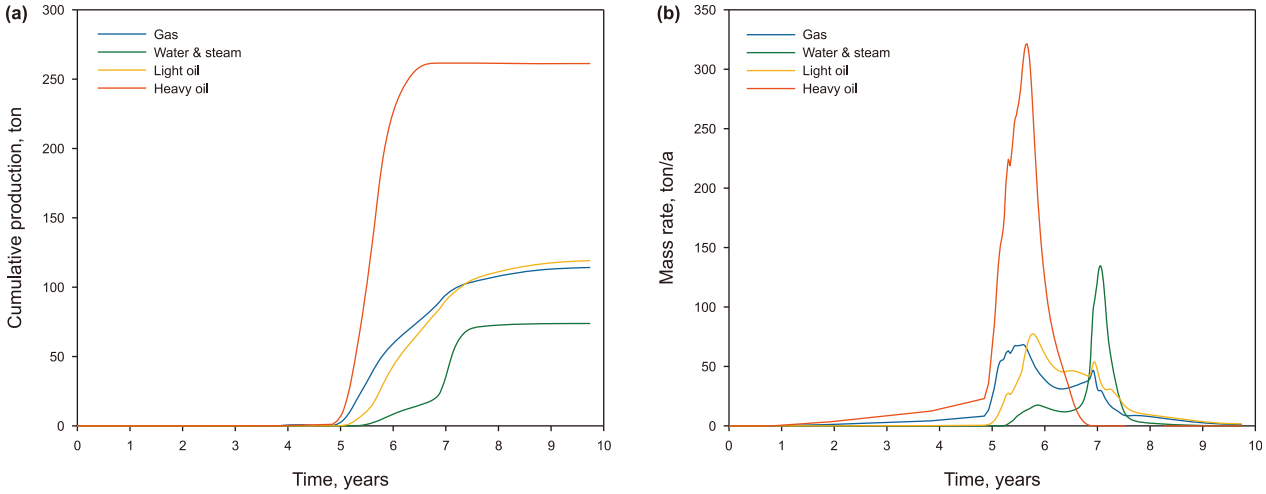

Fig. 7. **(a)** Cumulative mass of fluid production and **(b)** fluid production rate over time during in-situ conversion process.

naturally highly developed continental shale with abundant fractures, the reservoir's permeability is primarily controlled by the activated fracture's permeability (AFP). In general, the flow capacity of fractures can be calculated using the cubic law. However, it is challenging to determine the aperture of fractures accurately when numerous fractures are present. In addition, due to the often tortuous and rough nature of fracture surfaces, there can be significant differences between the hydraulic aperture that governs fracture flow and the mechanical aperture calculated based on stress equilibrium. Therefore, assessing the increase in permeability resulting from fracture activation is quite demanding. Hence, this study treats AFP as a variable and investigates the impact of AFP on the in-situ conversion process. For this purpose, injection is maintained at a constant heating power of 19.5 kW, and a cumulative 10-year heating development process is calculated for various levels of activated fracture permeability. This allows us to observe the effects of AFP on the in-situ conversion process and hydrocarbon production.

First, from the computational results, higher AFP indeed enhances fluid production. From Fig. 8, it becomes evident that the total production mass of fluids increases initially with higher AFP. However, as the AFP increases, the increment in total production mass varies for each fluid type and becomes smaller. Fig. 9 shows that when the AFP is greater than 1.0 mD, the total production mass of hydrocarbons is almost independent of AFP. This indicates that, over a 10-year development period, AFP exceeding 1.0 mD is no longer the bottleneck for fluid production.

Secondly, as denoted above, AFP has different effects on the production of different fluids. For heavy hydrocarbons, Fig. 8(a) and (b) demonstrate that high AFP enhances heavy oil production. With the increase in AFP, the final production mass of heavy oil after 10 years gradually increases. However, after the AFP exceeds 1.0 mD, the further increase no longer significantly promotes heavy oil production. Furthermore, when comparing the saturation distribution of heavy oil under different AFP conditions at the same moment, as depicted in subplots in Fig. 8(a), higher AFP leads to lower residual saturation of heavy oil in the reservoir. The main reason for the promotion of heavy oil production by increased AFP lies in the high viscosity of heavy oil, which creates a significant flow resistance and acts as the primary bottleneck in heavy oil production. Therefore, increased AFP proves advantageous for heavy oil production.

The effect of AFP on the production of light oil and natural gas differs significantly from its effect on heavy oil. Since the total mass of hydrocarbon fluids in the reservoir is fixed, and heavy oil can be cracked to form light oil and natural gas, to some extent, the production of heavy components and light components competes. As AFP increases, heavy oil production rises, which in turn diminishes the quality of light oil and natural gas generated through cracking, resulting in a decline in the cumulative production mass of light oil and natural gas with increasing AFP. This result also indicates that the primary bottleneck in the production of light oil and natural gas is not AFP, but rather the availability of a sufficient amount of heavy oil to crack during heating. Observing the cumulative production curves of light oil and natural gas, as shown in Fig. 8(d) and (f), a reduction in AFP delays the onset of fluid production; however, once production begins, higher production rates can be maintained. It is noteworthy that the sustained higher rates are contingent upon maintaining the reservoir's energy at an appropriate level. Since, as mentioned in the previous section and seen in Fig. 9, high AFP leads to a decrease in the reservoir's energy, limiting the effective production of light hydrocarbons, as observed in the saturation distribution subplots (Fig. 8(c) and (e)). Therefore, appropriately reducing AFP proves beneficial for the generation of light components, leading to the production of more light oil and natural gas.

In summary, AFP plays a pivotal role in both fluid production and heavy oil upgrading processes. Low AFP not only promotes the saturation of light hydrocarbons but also contributes to maintaining reservoir energy. Consequently, it is recommended to avoid heavy oil production simultaneously with treatment to promote heavy oil upgrading, increase reservoir pressure, and promote the activation of fracture. These findings align with the conclusions of Shi et al. (2023) regarding the benefits of maintaining high pressures during injection before initiating production, which facilitates oil exploitation. Once the pressure has significantly increased and a considerable injection time has elapsed, the production of light hydrocarbons can be initiated to maximize fluid production and quality.

4.3. Effects of heating power

Since heat injection is the fundamental driving force for in-situ conversion of continental shale, it is undoubtedly clear that the amount of heat input will inevitably have an impact on in-situ conversion. In this research, a constant heating power is employed to maintain the shale at an optimal temperature for efficient and controlled kerogen decomposition. To analyze the impact of different energy inputs on resulting production, a

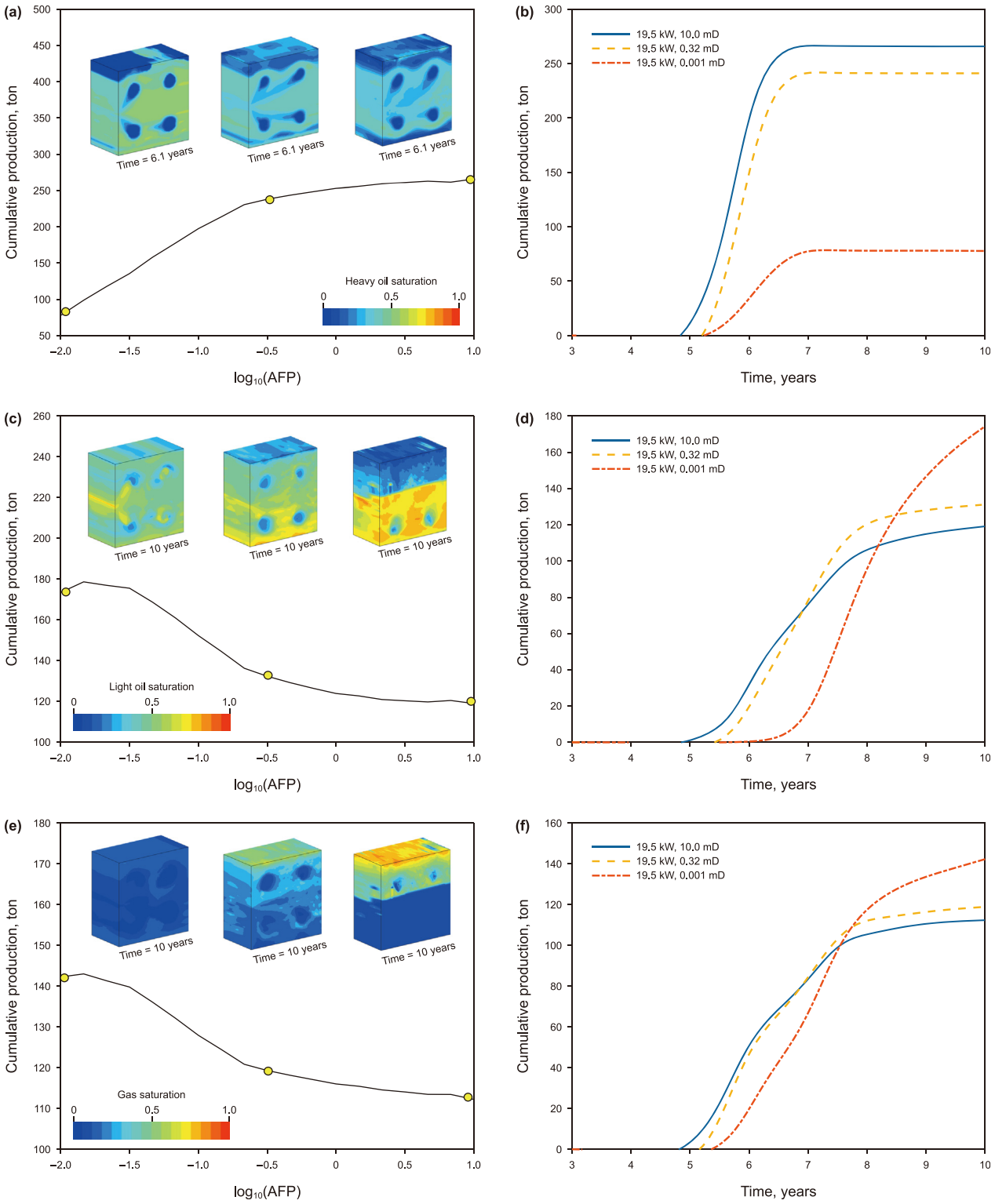

Fig. 8. Cumulative mass production of **(a)** heavy oil, **(c)** light oil, and **(e)** methane gas as a function of AFP in mD, along with cumulative mass production of **(b)** heavy oil, **(d)** light oil, and **(f)** methane gas over time under different AFP conditions. Insets in **(a)**, **(c)**, and **(e)** illustrate the three-dimensional saturation fields of fluids at typical times (time labels below the insets) corresponding to permeability conditions marked by circles on the curves. All results correspond to a heating power of 19.5 kW.

sensitivity analysis is conducted. The simulations are performed with an AFP of 10.0 mD.

The results indicate that the cumulative hydrocarbon production increases significantly with higher heating power levels, demonstrating a strong correlation between temperature and chemical decomposition. Specifically, the results shown in Fig. 10(b), (d), and (f) illustrate that temperature increases lead to higher fluid production and directly influence the onset of production. As the heating power increases, the temperature within the reservoir evolves more rapidly, reaching the producing wells

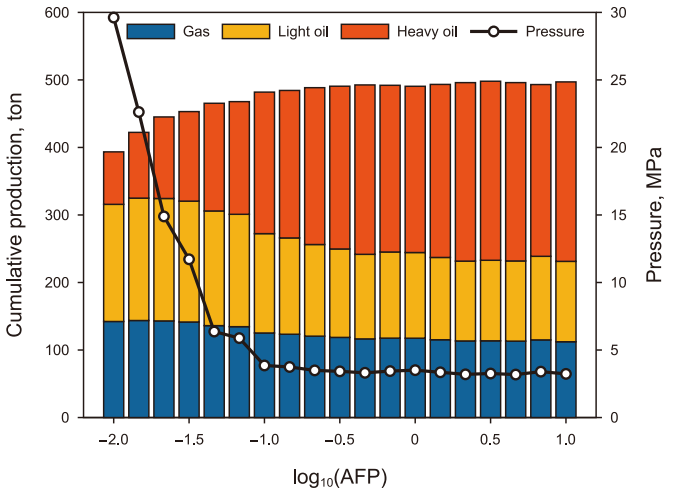

Fig. 9. Effects of AFP in mD on cumulative production distribution and final reservoir pressure. Each bar denotes the cumulative production of gas, light oil, and heavy oil, providing a comprehensive view of hydrocarbon distribution. Additionally, the plot includes a line graph depicting the final reservoir pressure corresponding to each fracture permeability.

more quickly and allowing for improved flow mobility (Briceño et al., 2023).

Furthermore, cumulative production reaches a satisfactory level at a heating power of 14 kW, where the average reservoir temperature exceeds 580 K, surpassing the decomposition temperature threshold (Fig. 11). While heat injection continues beyond 16.5 kW, increasing cumulative production, it becomes evident that the rate of production growth slows considerably. This deceleration can be attributed to the complete decomposition of kerogen. Remarkably, as the heating power exceeds 17 kW, heavy oil production experiences a noticeable decline (Fig. 10(a)). This decline occurs because the elevated temperatures at this energy level surpass the heavy oil cracking temperature, leading to increased saturation of light hydrocarbons (as shown in the subplots in Fig. 10(c) and (d)). Essentially, despite the production slowdown due to complete kerogen decomposition, the continued heat injection promotes heavy oil cracking, resulting in increased saturation of light hydrocarbons.

In summary, the findings underscore the importance of achieving a delicate balance in heating power within the reservoir. Sufficient heating power is required to initiate kerogen decomposition, but a critical temperature threshold exists that, once exceeded, can significantly enhance the oil quality, leading to increased production of lighter hydrocarbons. However, it is crucial not to surpass this threshold, as excess energy becomes redundant and results in energy wastage.

4.4. Comprehensive mode analysis

In the previous sections, the primary roles of AFP (the activated fracture's permeability) and heat injection in thermal recovery have been established. AFP defines the channels for fluid conduction resulting from decomposition to the production well, while temperature changes provide the energy necessary to initiate chemical reactions. To provide a more detailed analysis of the effects of AFP and heat injection, the cumulative production variations of the products obtained by combining both parameters are investigated. To achieve this, over four hundred cases are simulated.

The results are presented graphically in Fig. 12(a)–(d). The *x* and *y* coordinates represent AFP and heating power, respectively, while the *z* coordinates and the color of the surface represent cumulative production. From these results, four distinct modes of the in-situ conversion process emerge with varying heat power and fracture permeability.

1) *Ineffective heating mode.* In our analysis of the effects of AFP and heating power, a critical observation emerges regarding the heating power's impact. At an AFP of 10.0 mD and a development period of 10 years, a threshold heating power exists where there is no fluid conversion and production. This means that a heat injection below this power will not provide the energy necessary to achieve the minimum temperature for the decomposition of the components. It is evident that a heating power threshold exists under different AFP conditions, and this minimum injection remains almost the same across varying AFP conditions. In the context of this study, this threshold is approximately 13 kW. When heating power is below this threshold, the cumulative production of natural gas, light oil, or heavy oil is nearly zero. Therefore, regardless of reservoir conditions, in-situ conversion development must ensure a certain heating power as a prerequisite for fluid conversion and production.
2) *Heavy oil optimal mode.* Earlier analyses of AFP have suggested that higher AFP generally favors heavy oil production. However, through comprehensive analysis becomes apparent that the influence of AFP is not consistent across different heating power levels. Specifically, when heating power slightly surpasses the critical threshold and AFP is relatively high, it becomes most favorable to heavy oil production. Conversely, in scenarios with low AFP, heavy oil mobility is insufficient. Additionally, excessive heating power leads to increased cracking of heavy oil into light oil and natural gas. Both conditions contribute to a reduction in heavy oil production to some extent.
3) *Light oil optimal mode.* In the same context, the analysis of AFP indicated that relatively low AFP is favorable for light oil and natural gas production. The comprehensive analysis shows that, under different heating power levels, the effect of AFP is not uniform. Specifically, when heating power exceeds the critical power by a certain margin, and AFP is relatively low, it is most favorable for light oil and natural gas production. Conversely, if AFP is high, more heavy oil is produced, leading to a decrease in the amount of light oil and natural gas generated. If heating power is too low, the energy required for heavy oil cracking is insufficient. In both cases, light oil and natural gas production is reduced to some extent.
4) *Competing mode.* In cases where the production threshold is exceeded by heating power and does not align with either the heavy oil optimal mode or the light oil optimal mode, it can be defined as a competing mode. Under the conditions of the competing mode, neither heavy oil nor light fluids are produced under the most favorable conditions. This competing mode can be further divided into two sub-regions, each governed by its own unique mechanisms. It is observed that in these two sub-regions, when both AFP and heating power are relatively high, heavy oil production is favored by the high AFP, but higher heating promotes the cracking of heavy oil into light components. Alternatively, when AFP and heating power are relatively low, low AFP is conducive to light component production, but low heating power is unfavorable for heavy oil cracking.

It is important to note that this classification of modes just represents a trend. The heavy oil priority mode does not necessarily mean that more heavy oil is produced than light oil, but rather that it is the optimal mode for heavy oil development. Similarly, the light oil priority mode does not necessarily mean that the quality of

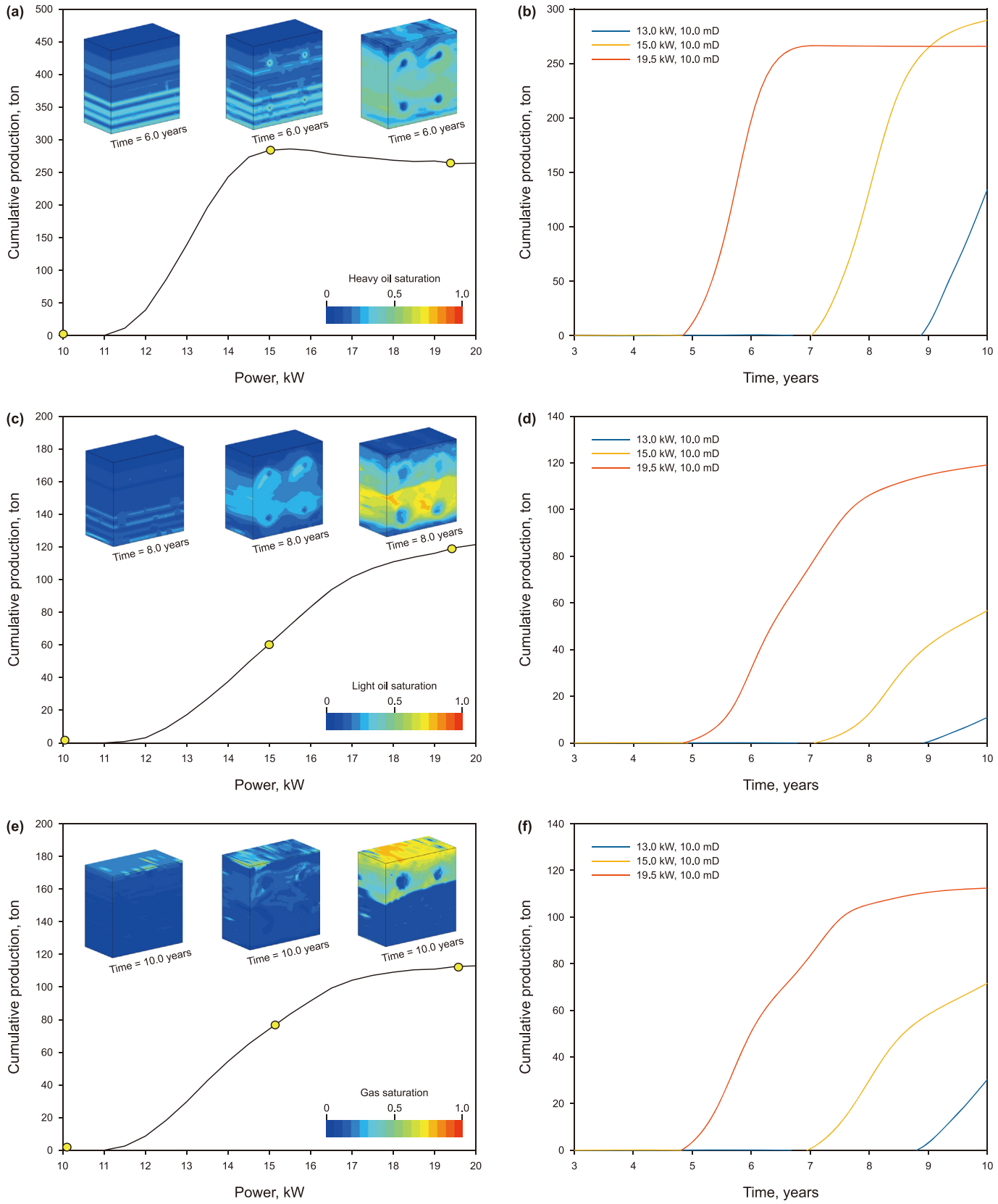

Fig. 10. Cumulative mass production of **(a)** heavy oil, **(c)** light oil, and **(e)** methane gas vs. heating power curves, and **(b)** cumulative mass production of heavy oil, **(d)** light oil, and **(f)** methane gas vs. time curves under different heating power conditions. The insets in figures **(a)**, **(c)**, and **(e)** depict three-dimensional saturation fields of fluids at typical times (times marked below the insets) corresponding to the heating power conditions marked with circles on the curves. All results correspond to an AFP of 10 mD.

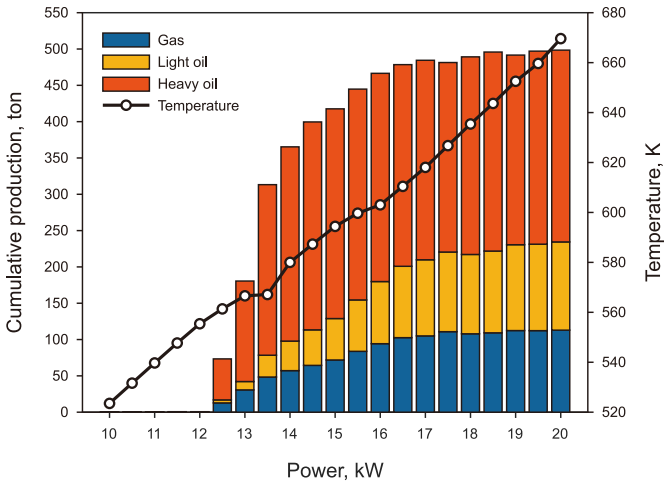

Fig. 11. Effects of power injection variation on cumulative production distribution and final reservoir temperature. Each bar represents the cumulative production of gas, light oil, and heavy oil, offering a comprehensive insight into hydrocarbon distribution. Additionally, the plot features a line graph illustrating the final reservoir temperature corresponding to each power injection scenario.

the produced light oil and gas components is greater than that of heavy oil. Additionally, in the coordinate system composed of AFP and heating power, there are no clear boundaries between these modes.

In summary, under different AFP conditions, the in-situ conversion process exhibits these four modes with varying heating power. First, it is crucial to avoid falling into the ineffective heating mode. Second, under effective heating conditions, if the goal is to produce more heavy oil, heating power should be reduced appropriately, and fluids should be produced as quickly as possible. Conversely, if the goal is to produce more light oil and natural gas, heating power should be increased, and shut-in periods should be applied to allow more time for heavy oil cracking.

4.5. Energy efficiency

The goal of in-situ conversion for oil and gas development is to obtain energy, but the heating process itself consumes a significant amount of energy. Therefore, to assess the feasibility of this in-situ conversion approach, it is essential to analyze energy utilization efficiency. Fan et al. (2010) proposed an efficiency measure for the in-situ method, quantified by the external energy ratio (*EER*), as introduced by Brandt (2008).

$$EER = \frac{E_{out}}{E_{in}} \tag{17}$$

In this context, E_{out} represents the higher heating value of the final refined product output, calculated by multiplying the final mass production of gas, light oil, and heavy oil for each simulation

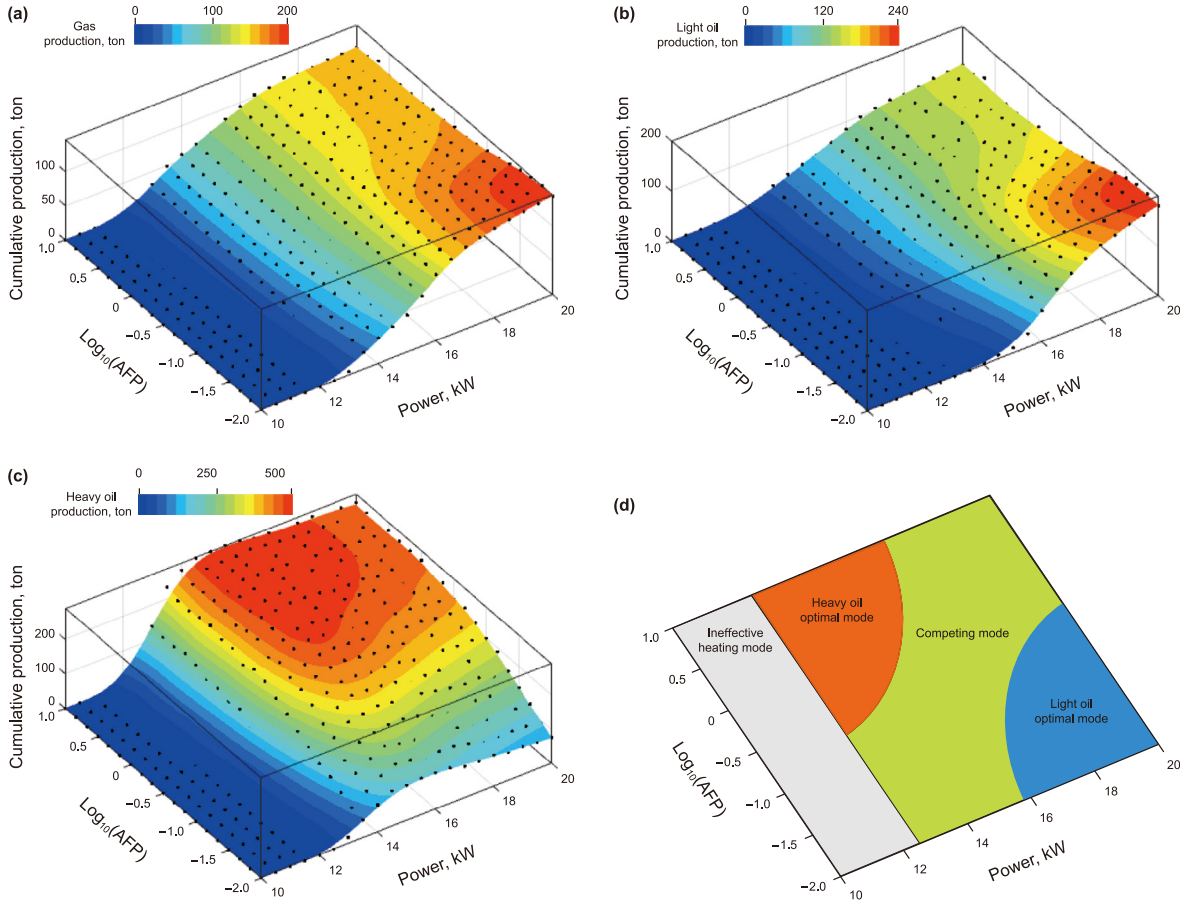

Fig. 12. After 10 years of in-situ conversion development, trends in the mass of **(a)** methane gas, **(b)** light oil, **(c)** heavy oil as a function of heating power and AFP in mD. Each small black dot in the figure represents a computational case, while the colored surfaces represent results smoothed based on these cases. **(d)** Presents a dimensional surface illustrating the four different modes that emerge with the variation of fracture permeability and injection power, providing a conclusive overview integrating the findings from the first three plots.

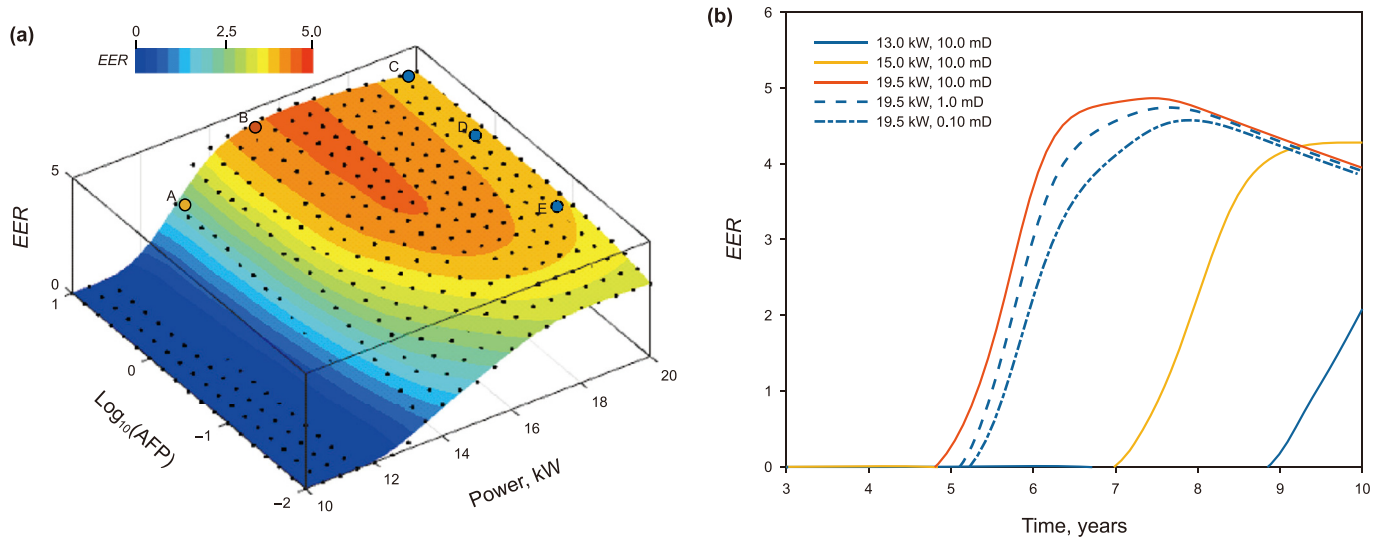

Fig. 13. **(a)** Trends in the energy utilization efficiency of in-situ conversion development as a function of heating power and AFP in mD. Each small black dot in the figure represents a computational case, while the colored surfaces represent results smoothed based on these cases. **(b)** Time-dependent variations in energy utilization efficiency under different heating power and reservoir permeability conditions.

case by their respective heat values. These heat values, derived from the standard heat released during combustion (World Nuclear Association, 2023), typically range from 55 MJ/kg for gas to 47 MJ/kg for liquid oil. While E_{in} represents the primary energy input from the external energy system, computed by multiplying the power injected by the simulation time. In their studies, Fan et al. (2010) and Huang et al. (2023) focused on analyzing efficiency ratios using a hexagonal injection pattern of the shell ICP method, assuming a 90% recovery efficiency of the system. In contrast, our research determines the energy efficiency ratio based on the cumulative production of various hydrocarbons (heavy oil, light oil, and gas) achieved in each simulation case.

Overall, except in cases of *ineffective heating mode,* the *EER* for in-situ conversion is about 4 (Fig. 13). In simpler terms, for each unit of energy used for heating, theoretically, around 4.0 units of heat are produced during fluid combustion. Specifically, when the heating power slightly exceeds the critical level, and the reservoir fracture permeability is high, as seen in the *heavy oil optimal mode*, the *EER* is highest, reaching around 5. Moreover, since in-situ conversion can handle short-term fluctuations in heating power, it can effectively use waste energy from wind and solar sources, which is almost cost-free. Therefore, economically speaking, this method of using waste energy for heating is feasible.

Furthermore, to simplify the calculations, continuous heat injection at a constant power level is assumed over a 10-year period of hydrocarbon production. However, through our analysis, considering the effects of heating power and referencing the findings of Shi et al. (2023) on injection energy and productivity, it is revealed that maintaining constant injection energy may not be necessary throughout the entire treatment duration. This is attributed that the decomposition of kerogen occurs at earlier stages, leading to a reduction in required energy input over time. A more effective strategy would involve applying higher power heating in the early stages of in-situ conversion and subsequently lowering the heating power as the temperature reaches the point of kerogen and heavy oil cracking. As shown in Fig. 13(b), under different conditions, the *EER* exhibits an initial ascent followed by a subsequent decline over time, indicating that continued heating beyond a certain stage does not yield additional benefits. Therefore, in the design of the actual in-situ conversion process, it is crucial to consider using different heating powers at different stages. Such an optimization strategy will result in higher energy utilization efficiency than the values predicted in this paper.

Consequently, the actual injection energy input in practical applications is lower than what was simulated, suggesting that the presented *EER* values are underestimated. Recognizing this observation is essential as it underscores the potential for even greater energy efficiency in real-world implementations of the in-situ conversion method. These insights provide valuable guidance for optimizing the energy input strategy, contributing to a more accurate evaluation of the method's overall efficiency and applicability in the context of sustainable energy practices.

In summary, this in-situ development method for continental shale oil is feasible in terms of energy utilization. Additionally, when considering the utilization of waste energy and the potential improvement in energy utilization efficiency through the optimization of injection power over time, this in-situ conversion method has the potential to become a promising approach for future continental shale oil development.

5. Conclusions

In-situ conversion is one of the potential methods for developing shale oil in continental shale reservoirs. However, the significant energy requirements associated with this approach pose challenges to its implementation. To address this issue, this research proposes a scheme to employ excess energy from wind and solar sources to provide heating within the reservoir, thereby rendering this method more feasible. Hence, assuming the implementation of this approach, a three-dimensional heterogeneous computational model, considering natural fractures, has been developed. Based on this model, the paper investigates the characteristics of phase evolution and optimization strategies for in-situ transformation during the heating process. The primary conclusions are as follows:

Firstly, an analysis of the entire life cycle of in-situ conversion development was conducted. It was observed that the stages of heating, reaction, and production do not occur simultaneously, but can be roughly categorized in terms of time as the heating stage, reaction stage, and production stage. In the reaction stage,

decomposition leads to an increase in fluid pressure, which in turn activates fractures. Fracture activation is a critical factor in ensuring reservoir permeability during subsequent production stages. Additionally, after a sufficiently long period of heating development, reservoir fluids have three possible fates: thermal cracking (mainly including kerogen and heavy oil), production (light oil, natural gas, water), and pore residuals (coke and light oil).

Secondly, the paper clarifies the roles of activated fracture's permeability (AFP) and heating power in the in-situ conversion process. In general, bigger AFP is advantageous for overall production and for boosting heavy oil production but may suppress light oil and natural gas production. On the other hand, increasing heating power is favorable for light oil and natural gas production. However, in-situ conversion only takes place when the heating power exceeds the minimum power to surpass the temperature of decomposition.

Thirdly, a comprehensive analysis of the effects of AFP and heating power reveals four in-situ conversion modes in a coordinate system formed by these two factors: *ineffective heating mode*, *heavy oil optimal mode*, *light oil optimal mode*, and *competing mode*. During production, it is essential to avoid falling into the *ineffective heating mode*. To obtain more heavy oil, it is advisable to increase permeability and maintain low heating power to make it in the *heavy oil optimal mode*. For those aiming to acquire more light oil and natural gas, production should be delayed to some extent, and heating power should be increased to make it in the *light oil optimal mode*.

Finally, the energy utilization efficiency of in-situ conversion under different conditions is analyzed. Under the condition of injecting one unit of energy, in-situ conversion can develop approximately 4.0 units of energy. Considering that, the injected energy comes from wasted wind and solar energy, the in-situ conversion method is feasible in terms of energy utilization.

In summary, this paper provides a quantitative analysis of the in-situ conversion production process through numerical simulations, focusing on a particular reservoir. While specific numerical values, such as heating power and production rates, may not be directly applicable to other reservoirs, the patterns revealed are universal and enhance our comprehension of the in-situ conversion process.

CRediT authorship contribution statement

Zhao-Bin Zhang: Writing – review & editing, Supervision, Software, Methodology, Data curation, Conceptualization. **Maryelin Josefina Briceño Montilla:** Writing – original draft, Visualization, Methodology, Investigation, Formal analysis, Conceptualization. **Shou-Ding Li:** Supervision. **Xiao Li:** Supervision. **Jian-Peng Xing:** Validation. **Yan-Zhi Hu:** Visualization.

Declaration of competing interest

The authors declare that they have no known competing financial interests or personal relationships that could have appeared to influence the work reported in this paper.

Acknowledgement

This research is supported by the National Natural Science Foundation of China (Grant No. 42090023), the Alliance of International Science Organization (ANSO) Scholarship for Young Talents, the Key Deployment Program of Chinese Academy of Sciences (YJKYYQ20190043, ZDBS-LY-DQC003, KFZD-SW-422, ZDRW-ZS-2021-3-1), the Scientific Research and Technology Development Project of China National Petroleum Corporation (2022DJ5503), the CAS Key Technology Talent Program, and Supercomputing Laboratory, IGGCAS.

References

Bai, Y., Ma, Y., 2020. Geology of the Chang 7 Member oil shale of the Yanchang Formation of the Ordos Basin in Central North China. J. Pet. Geosci. 26 (2), 355–371. https://doi.org/10.1144/petgeo2018-091.

Boak, J., Kleinberg, R., 2020. Shale gas, tight oil, shale oil and hydraulic fracturing. In: Letcher, T. (Ed.), Future Energy: Improved, Sustainable and Clean Options for Our Planet, third ed. Elsevier, pp. 67–95. https://doi.org/10.1016/B978-0-08-102886-5.00004-9.

Brandt, A.R., 2008. Converting oil shale to liquid fuels with the Alberta Taciuk Processor: energy inputs and greenhouse gas emissions. J. Environ. Sci. Technol. 4219, 6253–6258. https://doi.org/10.1021/ef900678d.

Braun, R., Burnham, A.K., 1993. Chemical Reaction Model for Oil and Gas Generation from Type I and Type II Kerogen. Lawrence Livermore National Laboratory, Livermore, CA, USA. https://doi.org/10.2172/10169154.

Briceño, M., Li, S., Zhang, Z., et al., 2023. Theoretical analysis of the effect of electrical heat in situ injection on the kerogen decomposition for the development of shale oil deposits. J. Energies 16 (5007), 1–23. https://doi.org/10.3390/en16135007.

Burnham, A.K., Braun, R.L., 1985. General kinetic model of oil shale pyrolysis. J. In Situ. 91, 1–23.

CMG Software | STARS, 2023. https://www.cmgl.ca/stars. (Accessed 31 August 2023).

Coal-Classification, 2023. https://www.engineeringtoolbox.com/classification-coal-d_164.html. (Accessed 4 January 2023).

Dang, S., Sondergeld, C.H., Rai, C.S., 2016. A new approach to measuring organic density. J. Petrophysics 57 (2), 112–120. SPWLA-2016-v57n2a3.

Darcy, H., 1856. Les fontaines publiques de la ville de Dijon. Victor Dalmont, Paris. https://books.google.com/books?id=42EUAAAAQAAJ (in French).

Egboga, N.U., Mohanty, K.K., Balhoff, M.T., 2017. A feasibility study of thermal stimulation in unconventional shale reservoirs. J. Petrol. Sci. Eng. 154, 576–588. https://doi.org/10.1016/j.petrol.2016.10.041.

Espitalie, J., Madec, M., Tissot, B., et al., 1977. Source rock characterization method for petroleum exploration. In: The Annual Offshore Technology Conference. https://doi.org/10.4043/2935-ms.

Fan, Y., Durlofsky, L.J., Tchelepi, H.A., 2010. Numerical simulation of the in-situ upgrading of oil shale. SPE J. 152, 368–381. https://doi.org/10.2118/118958-PA.

Fowler, T.D., Vinegar, H.J., 2009. Oil shale ICP - Colorado field pilots. In: SPE Western Regional Meeting. https://doi.org/10.2118/121164-ms.

Fu, J., Li, S., Xu, L., et al., 2018. Geological characteristic and exploration of shale oil in Chang 7 member of triassic yanchang formation, Ordos Basin, NW China. J. Pet. Explor. Dev. 456, 936–946. https://doi.org/10.11698/PED.2018.06.02.

Gischig, V., Preisig, G., 2015. Hydro fracturing versus hydro shearing: a critical assessment of two distinct reservoir stimulation mechanisms. In: The 13th International Congress of Rock Mechanics (ISRM). https://doi.org/10.13140/RG.2.1.4924.3041.

Guo, W., Yang, Q., Deng, S., et al., 2022. Experimental study of the autothermic pyrolysis in-situ conversion process ATS for oil shale recovery. J. Energy 258, 124–878. https://doi.org/10.1016/j.energy.2022.124878.

Hazra, K.G., 2014. Comparison of Heating Methods for In-Situ Oil Shale Extraction Master Thesis. Texas A&M University, Texas, USA, pp. 1–94. https://core.ac.uk/download/pdf/147240368.pdf.

He, J., Deng, H., Ma, R., et al., 2020. Reservoir characteristics of the lower Jurassic lacustrine shale in the eastern Sichuan basin and its effect on gas properties: an integrated approach. J. Energies 13 (17). https://doi.org/10.3390/en13174495.

Huang, H.W., Yu, H., Xu, W.L., et al., 2023. A coupled thermo-hydro-mechanical-chemical model for production performance of oil shale reservoirs during in-situ conversion process. J. Energy 268, 126–700. https://doi.org/10.1016/j.energy.2023.126700.

Hu, S., Zhao, W., Hou, L., et al., 2020. Development potential and technical strategy of continental shale oil in China. J. Pet. Explor. Dev. 47 (4), 819–828. https://doi.org/10.11698/PED.2020.04.19.

Jia, C., Zou, C., Li, J., et al., 2016. Evaluation criteria, major types, characteristics and resource prospects of tight oil in China. J. Petroleum Research 1, 1–9. https://doi.org/10.1016/S2096-24951730026-1.

Lee, K., 2014. Rigorous Simulation Model of Kerogen Pyrolysis for the in Situ Upgrading of Oil Shales. PhD Thesis, Texas A&M University, Texas, USA, pp. 2–196. https://hdl.handle.net/1969.1/153864.

Lee, K., Moridis, G., Ehlig-Economides, C., 2015. A comprehensive simulation model of kerogen pyrolysis for the in-situ upgrading of oil shales. In: SPE Reservoir Simulation Symposium. https://doi.org/10.2118/173299-PA.

Lei, G., Li, Z., Yao, C., et al., 2016. Numerical simulation on oil shale in-situ upgrading by steam injection. In: IET Conference Publications. https://doi.org/10.1049/cp.2016.1369.

Li, D., Li, J., Zhang, B., et al., 2017. Formation characteristics and resource potential of Jurassic tight oil in Sichuan basin. J. Petroleum Research 2 (4), 301–314. https://doi.org/10.1016/j.ptlrs.2017.05.001.

Li, Y., Hu, W., Zhang, Z., et al., 2021. Numerical simulation of hydraulic fracturing process in a naturally fractured reservoir based on a discrete fracture network model. J. Struct. Geol. 147, 104–331. https://doi.org/10.1016/j.jsg.2021.104331.

Meng, Q., Hao, F., Tian, J., 2021. Origins of non-tectonic fractures in shale. Earth Sci. Rev. 222, 103–825. https://doi.org/10.1016/j.earscirev.2021.103825.
Pei, S., Huang, L., Zhang, L., et al., 2020. Experimental study on thermal cracking reactions of ultra-heavy oils during air injection assisted in-situ upgrading process. J. Pet. Sci. Eng. 195, 107–850. https://doi.org/10.1016/j.petrol.2020.107850.
Ryan, R.C., Fowler, T.D., Beer, G.L., Nair, V., 2010. Shell's in situ conversion process-from laboratory to field pilots. In: Ogunsola, O.I., Hartstein, A.M., Ogunsola, O. (Eds.), Oil Shale: A Solution to the Liquid Fuel Dilemma. American Chemical Society, Washington, DC, pp. 161–183. https://doi.org/10.1021/bk-2010-1032.ch009.
Shen, C., 2009. Reservoir simulation study of an in-situ conversion pilot of Green-River oil shale. In: The SPE Rocky Mountain Petroleum Technology Conference 2009, pp. 204–212. https://doi.org/10.2118/123142-MS.
Shi, Y., Zhang, Y., Song, X., et al., 2023. Injection energy utilization efficiency and production performance of oil shale in-situ exploitation. J. Energy 263, 125–714. https://doi.org/10.1016/j.energy.2022.125714.
Stone, H.L., 1970. Probability model for estimating three-phase relative permeability. J. Petrol. Technol. 22 (2), 214–218. https://doi.org/10.2118/2116-pa.
Thomson, G., 1946. The Antoine equation for vapor-pressure data. Chem. Rev. 38 (1), 1–39. https://doi.org/10.1021/cr60119a001.
Thoram, S., Ehlig-Economides, C., 2011. Heat transfer applications for the stimulated reservoir volume. In: The SPE Annual Technical Conference and Exhibition. https://doi.org/10.2118/146975-ms.
Turakhanov, A., Tsyshkova, A., Mukhina, E., et al., 2021. Cyclic subcritical water injection into Bazhenov oil shale: geochemical and petrophysical properties evolution due to hydrothermal exposure. J. Energies 14 (15). https://doi.org/10.3390/en14154570.
Wagner, W., Kretzschmar, H.J., 2019. International Steam Tables, third ed. Springer, Berlin Heidelberg. https://doi.org/10.1007/978-3-662-53219-5.
Wang, B., Liu, B., Sun, G., et al., 2021. Evaluation of the shale oil reservoir and the oil enrichment model for the first member of the Lucaogou Formation, Western Jimusaer Depression, Junggar Basin, NW China. ACS Omega 618, 12081–12098. https://doi.org/10.1021/acsomega.1c00756.
Wang, J., Xie, H.P., Matthai, S.K., et al., 2023. The role of natural fracture activation in hydraulic fracturing for deep unconventional geo-energy reservoir stimulation. J. Pet. Sci. 20 (4), 2141–2164. https://doi.org/10.1016/j.petsci.2023.01.007.
Wang, L., Su, J., Yang, D., 2022. Study on pyrolysis–mechanics–seepage behavior of oil shale in a closed system subject to real-time temperature variations. J. Mater. 15 (15). https://doi.org/10.3390/ma15155368.
Wang, Y., Chao, Q., Zhao, L., et al., 2022. Assessment of wind and photovoltaic power potential in China. Carbon Neutrality 11, 1–11. https://doi.org/10.1007/s43979-022-00020-w.
Wood, D.A., 2022. Shale kerogen kinetics from multiheating rate pyrolysis modeling with geological time-scale perspectives for petroleum generation. In: Sustainable Geoscience for Natural Gas Subsurface Systems. Elsevier Inc, pp. 159–195. https://doi.org/10.1016/B978-0-323-85465-8.00001-7.
World Nuclear Association, 2023. Heat values of various fuels. https://www.world-nuclear.org/information-library/facts-and-figures/heat-values-of-various-fuels.aspx. (Accessed 18 August 2023).
Xi, Z., 2022. Advances in resources research discussion on main controlling factors of shale oil enrichment and recoverability in Biyang Sag of Nanxiang Basin. J. Adv. Res. 2 (3), 77–86. https://doi.org/10.50908/arr.2.3.
Xue, L., Dai, C., Wang, L., et al., 2019. Analysis of thermal stimulation to enhance shale gas recovery through a novel conceptual model. J. Geofluids. https://doi.org/10.1155/2019/4084356.
Xu, T., Zhang, Z., Li, S., et al., 2021. Numerical evaluation of gas hydrate production performance of the depressurization and backfilling with in-situ supplemental heat method. ACS Omega 66, 12275–12286. https://doi.org/10.1021/acsomega.1c01143.
Yang, Z., Zou, C., Wu, S., et al., 2019. Formation, distribution and resource potential of the “sweet areas sections” of continental shale oil in China. J. Mar. Pet. Geol. 102, 48–60. https://doi.org/10.1016/j.marpetgeo.2018.11.049.
Yaws, L.C., 2003. Yaws' Handbook of Thermodynamic and Physical Properties of Chemical Compounds. Knovel. https://doi.org/www.knovel.com/knovel2/Toc.jsp.
Younglove, B.A., Ely, J.F., 1987. Thermophysical properties of fluids II: methane, ethane, propane, isobutene, and normal butane. J. Phys. Chem. Ref. 16 (4). https://doi.org/10.1063/1.555785.
Zhang, C., Zhu, D., Luo, Q., et al., 2017a. Major factors controlling fracture development in the Middle Permian Lucaogou Formation tight oil reservoir, Junggar Basin, NW China. J. Asian Earth Sci. 146, 279–295. https://doi.org/10.1016/j.jseaes.2017.04.032.
Zhang, W., Xie, L., Yang, W., et al., 2017b. Micro fractures and pores in lacustrine shales of the Upper Triassic Yanchang Chang7 Member, Ordos Basin, China. J. Pet. Sci. Eng. 156, 194–201. https://doi.org/10.1016/j.petrol.2017.03.044.
Zhang, Z., Li, X., He, J., et al., 2017c. Numerical study on the propagation of tensile and shear fracture network in naturally fractured shale reservoirs. J. Nat. Gas Sci. Eng. 37, 1–14. https://doi.org/10.1016/j.jngse.2016.11.031.
Zhang, Z., Li, Y., Li, S., et al., 2024. Optimization of the natural gas hydrate hot water injection production method: insights from numerical and phase equilibrium analysis. Appl. Energy 361 (3), 122963. https://doi.org/10.1016/j.apenergy.2024.122963.
Zhang, Z., Xu, T., Li, S., et al., 2023. Comprehensive effects of heat and flow on the methane hydrate dissociation in porous media. J. Energy 265. https://doi.org/10.1016/j.energy.2022.126425.
Zhao, B., Li, Y., Huang, W., et al., 2021. Experimental study on mechanical properties of shale rock and its strength criterion. Arabian J. Geosci. 14 (4). https://doi.org/10.1007/s12517-021-06552-2.
Zhao, W., Hu, S., Hou, L., 2018. Connotation and strategic role of in-situ conversion processing of shale oil underground in the onshore China. J. Pet. Explor. Dev. 45 (4), 537–545. https://doi.org/10.11698/PED.2018.04.01.
Zhao, W., Hu, S., Hou, L., et al., 2020. Types and resource potential of continental shale oil in China and its boundary with tight oil. J. Pet. Explor. Dev. 47 (1), 1–10. https://doi.org/10.11698/PED.2020.01.01.
Zhu, R., Zou, C., Mao, Z., et al., 2019. Characteristics and distribution of continental tight oil in China. J. Asian Earth Sci. 178, 37–51. https://doi.org/10.1016/j.jseaes.2018.07.020.
Zou, C., Yang, Z., Cui, J., et al., 2013. Formation mechanism, geological characteristics and development strategy of no marine shale oil in China. J. Pet. Explor. Dev. 40 (1), 15–27. https://doi.org/10.1016/S1876-38041360002-6.
Zou, C., Yang, Z., Sun, S., et al., 2020. “Exploring petroleum inside source kitchen”: shale oil and gas in Sichuan Basin. J. Sci. China Earth Sci 63 (7), 934–953. https://doi.org/10.1177/0144598717744066.